Energy & Buildings 295 (2023) 113233

Contents lists available at ScienceDirect

Energy & Buildings

journal homepage: www.elsevier.com/locate/enb

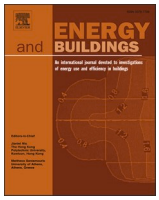

Building integrated vegetation effect on micro-climate conditions for urban heat island adaptation. Lesson learned from Turin and Rome case studies

Tiziana Susca *, Fabio Zanghirella, Vincenzo Del Fatto

ENEA - Italian National Agency for New Technologies, Energy and Sustainable Economic Development, Via Anguillarese, 301 - 00123 S. Maria di Galeria, Rome, Italy

ARTICLE INFO

Keywords:
Urban heat island
Green roof
Green wall
Green façade
Living wall
ENVI-met
Urban climate
Climate adaptation
Urban planning

ABSTRACT

The proposed study investigates the effect of urban heat island mitigation scenarios by applying extensive green roofs, green façades, and living walls to two built areas within Turin and Rome, Italy. Three mitigation scenarios and a baseline one have been developed in ENVI-met software for each built area and run for a typical winter day, summer day, and summer day with a heat wave.

The simulation results show that building integrated vegetation technology-application on a single building has an irrelevant effect on local temperatures; contrariwise, building integrated vegetation technology-wide application can effectively mitigate urban warming. Furthermore, the effect of green roofs and green walls on urban temperature is negligible in winter, likely because of the limited plant activity and the reduced amount of incoming solar radiation. Results also show that green façades are more effective than green roofs in mitigating pedestrian-level air temperature when installed on high-rise buildings, and green walls are more beneficial in mitigating summer urban heat island when installed in canyons parallel to wind direction than in perpendicular ones. Depending on the mitigation scenario, average decreases in urban temperatures up to 1 °C can be reached in the whole selected built area, alleviating urban warming.

1. Introduction

In 2016, urban areas covered 59.56 million hectares globally, representing 1.29% of the total Earth's surface occupied by built-up areas, grazing, and cropland [1], and the urban population was 54.4% of the global one [2]. The UN World Urbanization Prospects estimate that the global urban share population will reach 68.36% by 2050 [3], entailing further urbanization. Urbanization, in turn, modifies the natural thermal balance giving rise to an increase in surface and air urban temperature compared to the rural environs, known as Urban Heat Island (UHI) phenomenon [4]. Forecasts related to urban expansion scenarios reveal that under the current fossil-fueled development pathway, Europe will be exposed to an additional Surface UHI (SUHI)-warming equal to 0.12 °C in summer by 2100 [5].

Earth satellite-derived images are commonly used to detect SUHI from remote [6,7], which, in turn, is strictly correlated to atmospheric UHI [8,9] (hereafter UHI) and can be used to predict it. Both large- and medium-sized cities worldwide are plagued by urban overheating [10–12]. For instance, Manila and Mumbai are experiencing a rise in summer UHI intensity equal to 0.015 and 0.036 °C/decade, respectively, and in Beijing, the winter UHI intensity increases by 0.18 °C/decade [13].

The surge in urban temperature increases building energy use for summer cooling [14,15], contributes both directly and indirectly to air quality deterioration [16], and negatively affects human health [17]. Therefore, UHI mitigation is crucial to make cities "inclusive, safe, resilient and sustainable," contributing meeting the UN's 11th Sustainable Development Goal [18].

The increase in urban greening can limit UHI's environmental and societal negative effects [19–22]. In densely urbanized areas, buildings' surfaces (i.e., façades and rooftops) can offer room for the installation of vegetation that, otherwise, could hardly be added to the urban layout since residual spaces are often missing within cities. Specifically, Building Integrated Vegetation Technologies (BIVTs) such as green roofs and green walls can be installed, contributing to urban climate adaptation.

Both green roofs and green walls can be clustered into subcategories depending on the growing medium layer. Intensive green roofs (IGRs) are characterized by a growing medium layer whose thickness ranges from 15 to 120 cm [23], allowing shrubs and small trees to grow.

* Corresponding author.
E-mail addresses: tiziana.susca@enea.it (T. Susca), fabio.zanghirella@enea.it (F. Zanghirella), vincenzo.delfatto@enea.it (V. Del Fatto).

https://doi.org/10.1016/j.enbuild.2023.113233
Received 7 February 2023; Received in revised form 1 June 2023; Accepted 5 June 2023
Available online 13 June 2023

Extensive green roofs (EGRs) are characterized by a growing medium whose thickness is less than 12 cm, and they usually host small plants, typically sedum [22]. The growing medium for living walls (LWs) is vertically placed and adherent to the wall structure [24], while it is horizontal on the ground for green façade (GFs) [25]. In urbanized areas, the installation of green roofs is constrained to extensive ones, which differ from intensive ones for their limited weight (i.e., 50–150 kg m^{-2} at maximum water capacity vs. > 350 kg m^{-2} at maximum water capacity for IGRs) [26]. Both green roofs and green walls reduce air temperature and heat exchanges with buildings since vegetation can decrease up to 90% of the incoming solar radiation depending on leaf density through shading [27], reflect part of solar radiation because of their albedo [28], replace sensible heat with latent heat through evapotranspiration [29], and provide thermal insulation [30].

Although the effectiveness of green wall and green roof installation in reducing building energy needs for summer cooling—which, in turn, indirectly mitigates UHI—has been largely proven, the magnitude of direct UHI mitigation depends on climate, urban geometry, meteorological conditions, technology, scale of application and plant species [31,32].

In recent years, many modeling studies investigating the effect of green wall and green roof installation on UHI mitigation have been published [33–34]. Nevertheless, most published studies focus on a single aspect related to the interaction between BIVT installation and local climate. For instance, Ibrahim [36] compared the effect of three scenarios based on the single application of green roofs, green walls, and urban parks to detect which mitigates UHI to the greatest extent neglecting any speculation about other aspects such as the scale of application. Contrariwise, Herath et al. [37] explored both the effect of applying scenarios based on green roofs or green walls and the variation in plant coverage percentage, limiting the analyses to summer days. In addition, Shafiee et al. [38] only investigated the effect of LW installation on the UHI in Shiraz, Iran, to demonstrate its effectiveness in limiting urban warming. Albeit narrow investigations are interesting, their results about the behavior of the BIVT installation can hardly be generalizable, providing limited support to urban decision-making.

The present study contributes to filling such a scientific gap by reporting on the differences in urban microclimate conditions based on the application of multiple BIVT scenarios. Furthermore, the present study is innovative compared to published literature since, differently from previous research, it concomitantly investigates different crucial aspects (i.e., urban pattern, scale of application, BIVT typology, and effect on different seasons) about built environment-local climate interaction. To this aim, two densely urbanized areas featuring different layouts have been selected, one in Turin and the other in Rome. A baseline scenario and three UHI mitigation ones were defined for each urban area, and 3D models were developed and run in ENVI-met [39][1]—a three-dimensional microclimate model capable of simulating climatological interactions between surfaces, plants, and the atmosphere—considering the weather conditions of a typical summer day, a typical winter day, and a summer day with a heat wave. The investigation of the three typical days is innovative since most studies focus only on summer days. Specifically, the effect of UHI adaptation scenarios in heat wave days is not well-documented, although both heat waves and UHI are becoming more frequent and widespread phenomena [41], and their synergic effect can be a lethal threat to urban dwellers [42]. All in all, the proposed investigation provides broad climate-based information to support urban decision-making processes in UHI adaptation.

2. Materials and methods

We first investigated the SUHI to detect the two Italian cities with the greatest SUHI which, according to the adopted methodology, are Turin and Rome. Turin, and Rome are both characterized by a temperate climate according to Köppen-Geiger classification; specifically, Turin is classified as Cfa climate and Rome as Csa.

We investigated the effect of applying UHI mitigation scenarios for the two cities. In particular, the atmospheric UHI related to the urban canopy layer has been considered.

The main steps of the research are displayed in Fig. 1 and described in the following.

Step 1. For each of the two cities, a densely urbanized area (i.e., featured with an urban density index equal to 0.32 and 0.41 for Turin and Rome, respectively) prone to UHI formation and owing a meteorological station has been selected. Furthermore, we identified a weather station set at the airport or in a rural area. Table 1 displays relevant information and the urban and rural meteorological station position.

The georeferenced layers of the buildings within the two areas have been downloaded from the Italian Ministry of the Environment and the Protection of the Territory and the Sea Geoportal [47]. The approximate buildings' construction periods and the external buildings' finishing materials have been hypothesized from visual inspections employing Google Street View and Google Earth. Therefore, the stratigraphy of the buildings' envelopes has been attributed (Table B1). From visual inspection, the color of each urban surface has been acquired, and the corresponding albedo values have been retrieved from an online catalog [48]. Thus, thermophysical information about each material constituting the stratigraphy of the buildings' envelopes has been gathered and used to implement the ENVI-met database with the missing materials and the missing envelopes' components (i.e., rooftops and perimetral walls). Therefore, the stratigraphies of a perimetral wall and a rooftop have been associated to each building within the selected areas (Table B2, Table B3). Likewise, the urban surfaces' stratigraphy has been hypothesized (Table B4, Table B5) and implemented in ENVI-met database. Furthermore, Google Street View and Google Earth have been used to inspect the areas and gather information about vegetation position, species, tree crown dimension, and height. As for buildings' envelope components, a vegetation abacus has been developed (Table B6, Table B7), and the features of vegetation species have been implemented into the ENVI-met database when missing.

Step 2. Buildings, urban surfaces, and urban vegetation shapefiles have been created in QGIS®[49] to model the two urban areas and then implemented in ENVI-met. For the two urban areas, a grid of 3 m (x) × 3 m (y) × 3 m (z) has been chosen for the modeling since it can provide quite accurate outputs in an acceptable simulation time (i.e., about 48 h for a two-day simulation run with a processor Intel® Core (IM) i7-9700 CPU @3.00 GHz with a 32.0 GB RAM). Furthermore, as suggested by ENVI-met developers, additional grid cells have been added between the buildings and model borders to each modeled urban area to avoid the edge effect. Details about the developed ENVI-met models representing the baseline scenario are shown in Table 2.

Step 3. The historical datasets of the two urban meteorological stations have been used to select the typical winter day, summer day, and summer day with a heat wave for each city. Specifically, the months with the lowest and the highest average daily temperature values were

[1] Literature has been reviewed to detect the best tool for investigating the effect of UHI mitigation scenarios on urban climate. Mirzaei [40] clusters UHI modeling tools into microscale and urban-scale models, with micro-scale modeling tools which can be clustered into microclimate and urban canopy models. In the former, the computational fluid dynamics (CFD) technique computes the air flows around buildings; in the latter, the airflow model and the energy budget equation are distinguished. Urban-scale models integrate CFD techniques and models, including the interactions between solar radiation, cloud cover, and soil [40]. Typically, microscale models are preferred for assessing the local climate phenomena, for instance, within urban canyons, while mesoscale models are mainly used to assess urban-wide UHI mitigation measures such as urban policy plans [40]. Since the present investigation focuses on selected urban areas rather than the whole urban areas, a microclimate tool (i.e., ENVI-met) has been preferred for the simulations.

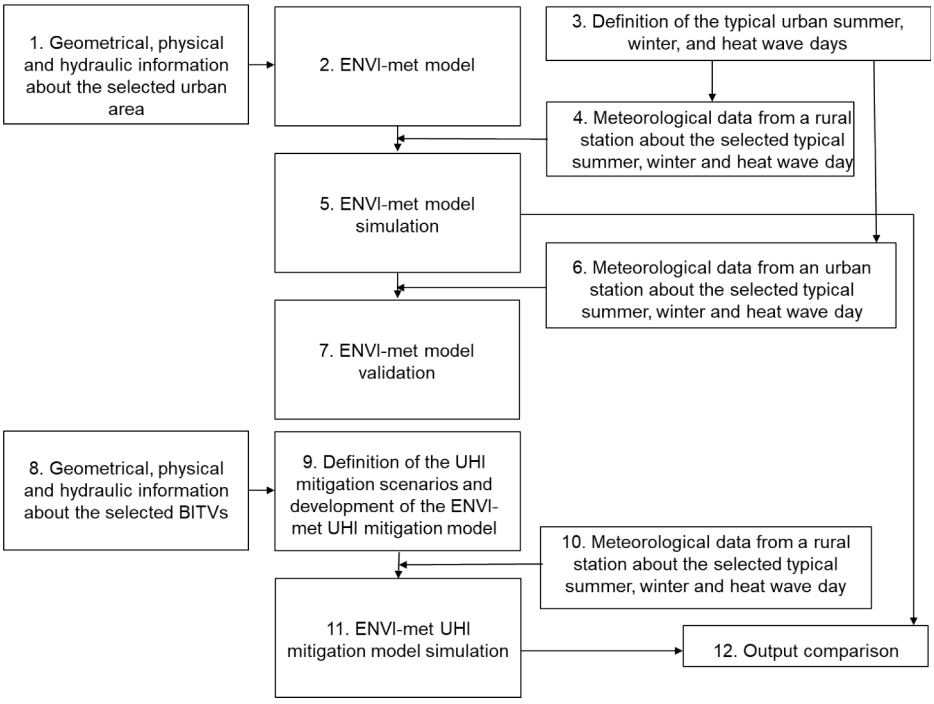

Fig. 1. Steps of the performed study.

identified using the Italian test reference year meteorological data (i.e., [50]). Then, the average hourly air temperature profiles were calculated for the selected months (see Figure C1 and Figure C2). The profiles were used as a reference for identifying the typical winter and summer days for Turin and Rome, among the not rainy days recorded by the urban weather stations (see Table C1, Table C2, Table C5 and Table C6). Besides, among the days reported as "heat wave" by the Italian National Center for Disease Prevention and Control of the Italian Ministry of Health, those with the highest apparent temperature (whose definition can be found in Appendix C) within the year with the highest number of heat wave days were selected [51,52] (see Table C9 and Table C10). Table 3 shows the winter, summer, and summer with heat wave typical days (for further details, see Appendix C).

Steps 4–5. For the above-mentioned typical days, the meteorological data have also been retrieved from the two rural stations (Table C3, Table C4, Table C7, Table C8, Table C11, and Table C12) and used to force the urban areas ENVI-met models. Specifically, air temperature, relative humidity, wind direction, and wind speed data were used to set up the boundary conditions within the ENVI-met simulations. Moreover, for the simulations of the selected urban area in Turin, the main wind direction (i.e., North-Northeast) was used (Table C13-Table C18). This latter has been retrieved from published literature [53].

Steps 6–7. The ENVI-met simulation outputs about the typical days have been compared with the meteorological data from the urban station to validate them (Figure E1).

Step 8. The stratigraphy of the materials constituting the BIVTs has been defined to develop the mitigation scenarios in ENVI-met. Subsequently, it was checked which of the materials of the BIVTs were missing in the ENVI-met database. The hydraulic and physical features of the missing materials were collected, modeled, and implemented within the database (Table 4). Next, the materials constituting the green roofs and the green walls have been assembled in the ENVI-met database to model the BIVTs. Whenever more than three materials constituted the stratigraphy of a BIVT, equivalent materials constituted by two or more materials have been modeled since ENVI-met does not allow including more than three materials for each building component (Table 4, see filter membrane and drainage layer for the extensive green roof).

Step 9. Three potential UHI mitigation scenarios based on the installation of EGRs, GFs, LWs, or a combination of two BIVTs have been developed for each urban area (Fig. 2) to evaluate the effect of the explored BIVTs, of the scale factor for their application, and the urban pattern. The scenarios have been identified with the abbreviations TO and RM when referring to urban areas in Turin and Rome, respectively. Specifically, the developed scenarios are (Fig. 2):

- Scenario TO1 - installation of LWs on the walls of an urban canyon approximately parallel to the main wind direction (i.e., North-Northeast). This latter has been retrieved from published literature (i.e., [53]);
- Scenario TO2 - installation of GFs on the walls of an urban canyon in a street approximately parallel to the main wind direction;
- Scenario TO3 - installation of LWs on the walls of an urban canyon in a street approximately perpendicular to the main wind direction;
- Scenario RM1 - broad installation of EGRs excluding the installation of green roofs on pitched rooftops;
- Scenario RM2 - broad installation of EGRs and GFs, excluding the installation of green roofs on pitched rooftops;
- Scenario RM3 – installation of GFs on a single building.

Specifically, scenarios TO1 and TO2 have been developed to test the difference in the effectiveness of LWs and GFs in mitigating UHI under the same conditions (i.e., urban context, orientation, wind direction, and wind speed); scenario TO3 has been developed to be compared with the outputs deriving from scenario TO1 to test the effect of canyon orientation where LWs are applied. In addition, scenarios RM1 and RM2 have been developed to compare the effect of the building height on EGR effectiveness in mitigating UHI and of GFs applied to high-rise buildings. Lastly, scenarios RM3 and RM2 have been developed to test the effect of the scale of application of GFs on UHI mitigation.

Steps 10–11. For the typical days, the meteorological data retrieved from the rural stations have been used to force the ENVI-met models of the UHI mitigation scenarios (Table C13-Table C18). Specifically, the ENVI-met models have run for 48 h for each typical day, with the 24 h before the typical days used for model initialization.

Step 12. The simulation outcomes of the UHI mitigation ENVI-met scenarios have been compared to those related to the baseline ones.

Table 1
Visualization of the rural and urban stations.

Turin[a]	Rome[a]
	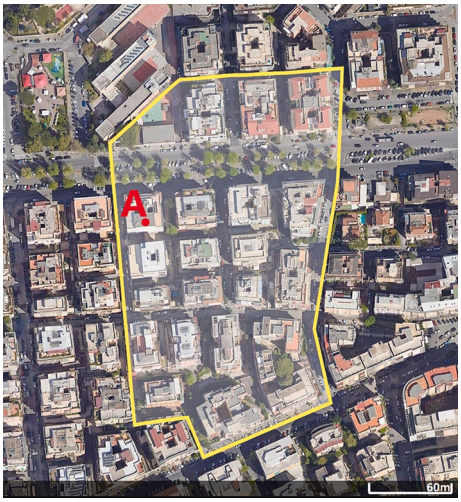
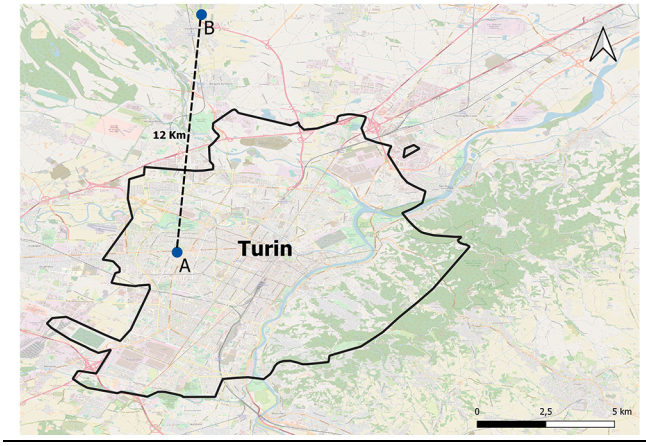	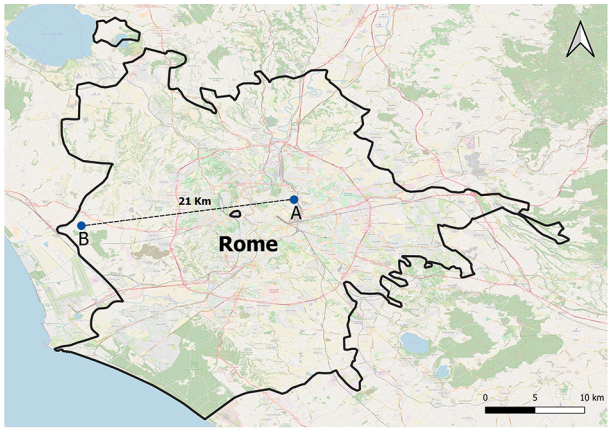

A = urban station
B = rural or airport station

Urban station: coordinates (altitude), address	Turin 45.074577 N, 7.638075 E (260 m a. s. l.), Beaulard street 7	Rome 41.920555 N, 12.523626 E (36 m a. s. l.), Lanciani street 38
Urban station: meteorological station model	Davis Vantage Pro2[b,g]	Campbell CR1000[c,h]
Urban station: data source	[43]	[44]
Rural or airport station: coordinates (altitude), location	45.18379 N, 7.64974 E (300 m a. s. l.), Caselle airport[d,i]	41.889451 N, 12.266327 E (61 m a. s. l.), Castel di Guido[e,i]
Rural station: data source	[45]	[46]
Urban layout	Enclosed[l]	Scattered[m]
Vegetation density[f]	0.19	0.05

[a] The yellow lines delimit the case-study domains, and the black lines delimit the borders of the two municipalities
[b] Installed on the rooftop of a 20 m high building
[c] Installed on the rooftop of a 20 m high building
[d] Installed at 1.6 to 10 m above the ground
[e] Installed at 2 m above the ground
[f] Vegetation density is calculated as the ratio between the surface occupied by urban vegetation within the urban area and the surface of the whole selected urban area
[g] The retrieved data from this meteorological station are: air temperature, relative humidity, wind speed, and solar radiation
[h] The retrieved data from this meteorological station are: air temperature, relative humidity, wind speed, wind direction, and solar radiation
[i] The retrieved data from this meteorological station are: air temperature, relative humidity, wind speed, and wind direction
[l] The enclosed urban pattern is featured by buildings forming closed polygons with internal courtyards
[m] The lack of physical continuity of the buildings characterizes the scattered urban layout

Table 2
Models of the baseline scenarios related to Turin (i.e., A) and Rome (i.e., B). Green tridimensional elements represent vegetation. Buildings are represented in grey in the urban area in Turin and with different colors in the urban area in Rome.

Features of the ENVI-met models of the urban areas	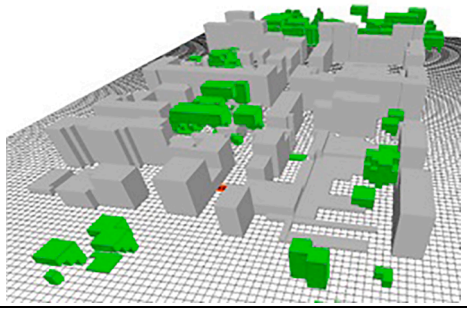	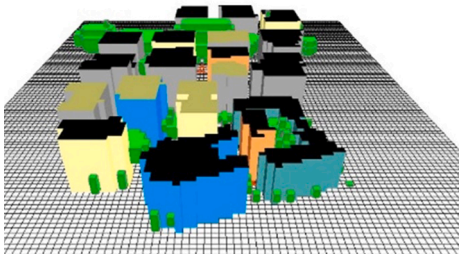
	A Turin baseline-scenario	B Rome baseline-scenario
Dimension of the urban areas (X × Y)	300 m × 400 *m*	270 m × 370 *m*
Dimension of the grid cells (X × Y × Z)	3 m × 3 m × 3 *m*	3 m × 3 m × 3 *m*
Added cells along X, Y, and Z axes	17	15
Z telescoping	30%	30%

Table 3
Typical days chosen for the ENVI-met simulations.

	Turin	Rome
Typical winter day	19/01/2016	19/02/2015
Typical summer day	27/07/2014	01/07/2015
Typical heat wave day	07/07/2015	22/07/2015

3. Results

3.1. UHI magnitude

The air temperature data retrieved from the urban and rural stations have been used to calculate the UHI magnitude for the typical days for both urban areas (Figure D1-Figure D2).

In Turin, the average UHI for the typical winter day (i.e., 19/01/2016) equals 2.4 °C and the peaks of 3.9 and 4.2 °C in the difference in temperatures are recorded at 11.00 am and at 10.00 pm, respectively. For the typical summer day (i.e., 27/07/2014), the average UHI equals 1.1 °C with a peak of 4.4 °C in the early morning hours. During a typical summer day with the heat wave, the average UHI magnitude equals 0.9 °C with peaks of 2.4 °C, 2 °C, 1.9 °C, and 1.6 °C at 06.00 am, at 00.00 am, at 11.00 am, and at 10.00 pm, respectively.

In Rome, for the typical winter day (i.e., 19/02/2015), the average UHI equals 0.4 °C with peaks of 1.5 and 1.0 °C at 3.00–3.30 am and 09.00 am, respectively. During the typical summer day (i.e., 01/07/2015), the average UHI equals 2.2 °C with peaks of 3.8 °C, 3.1 °C, and 2.9 °C at 06.30 am, 03.30 pm, and 10.00 pm, respectively. The average UHI during a heat wave (i.e., 22/07/2015) equals 1.4 °C with peaks of 4.2 °C, 3.8 °C, and 3.0 °C at 12.30 pm, 02.30 pm, and 10.00 pm, respectively.

By comparing the UHI magnitude in Turin and in Rome related to the typical day with a heat wave with that of a typical summer day, it can be noticed that the maximum UHI is similar for both typical days. Nevertheless, the UHI of a typical day with a heat wave can entail more negative effects than the UHI of a typical summer day since the average temperature during the typical day with a heat wave equals is higher than that of the typical summer day.

3.2. Model validation

Among the simulation software, ENVI-met has been chosen among the other microclimate modeling tools since, compared to other simulation software, it shows better accuracy in predicting air temperature [58]. Specifically, Szűcs et al. [59] found that the correlation coefficient between the simulated and measured air temperatures was 0.956, while Solweig and Rayman showed lower values equal to 0.866 and 0.867, respectively, showing that the simulation results provided by ENVI-met are more accurate than Solweig and Rayman. Moreover, ENVI-met has also been validated against other software, showing that it better predicts air temperatures than other software [60–62].

Model validation is vital to produce reliable simulation outputs [34], therefore, in the present study, temperatures related to the typical days recorded by the urban stations in the urban canopy layer in the selected urban areas in Turin and Rome (Table 1) were used to validate the outputs of the ENVI-met models. Specifically, for both the urban areas, baseline scenarios simulated air temperature values related to the test point where the meteorological stations are installed (i.e., at an altitude of 22.5 m above the ground) were compared with those retrieved by the two weather stations (see, Figure E1-Figure E6) to validate them. Furthermore, using recorded and simulated temperatures, Root Mean Square Error (RMSE) and Mean Absolute Error (MAE) were calculated for each typical day (Table 5) and compared with the RMSE and MAE values provided by Tsoka et al. [63].

Specifically, the data from a study by Tsoka et al. [63] about the RMSE and MAE between simulation air temperatures and recorded ones have been retrieved, divided according to summer and winter simulations, and presented in a boxplot. Table 5 shows that the RMSE and the MAE values found for the case studies of the present research are compatible and sometimes lower than those retrieved from Tsoka et al. [63]; therefore, they can be considered acceptable since they show a similar level of approximation.

3.3. Simulation numerical analyses: Air temperature

For both urban areas and each typical day, the hourly air temperature results of the simulations (i.e., both baseline and mitigation scenarios) related to 2.1 m above the ground (i.e., at pedestrian level) have been retrieved and used to calculate the spatially averaged hourly temperatures; these latter have been compared to calculate the hourly (Table E1) and daily (Table 6 lines 2–7) UHI mitigation values. Within the present study, we consider mitigation values between ± 0.2 °C as negligible since thermometers cannot detect such differences [64]; therefore, the mitigation scenarios exerting negligible air temperature reductions will not be discussed in detail in the following. Contrariwise, for each mitigation scenario, the hours with the greatest temperature mitigation (Table 6, lines 8–13) have been discussed in more detail.

Table 4
Hydraulic and physic characteristics of the layers of the BIVTs modeled in ENVI-met.

Extensive green roof
(ENVI-met identifier number: EXGR01)

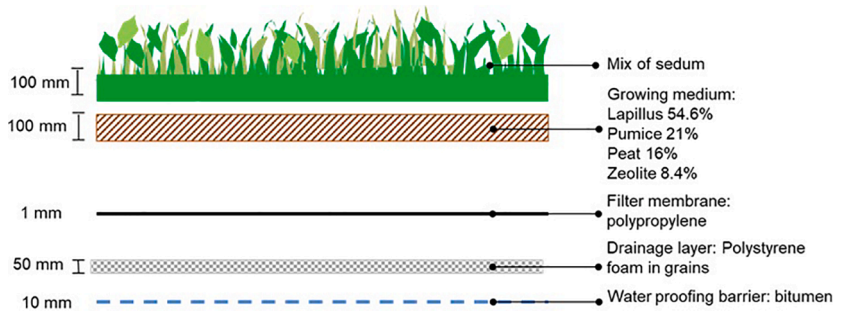

Green façade
(ENVI-met identifier number: GRFA01)

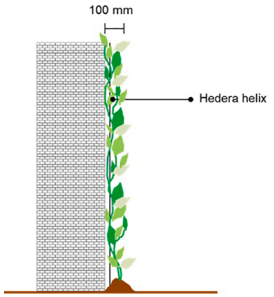

Living wall
(ENVI-met identifier number: LIVW01)

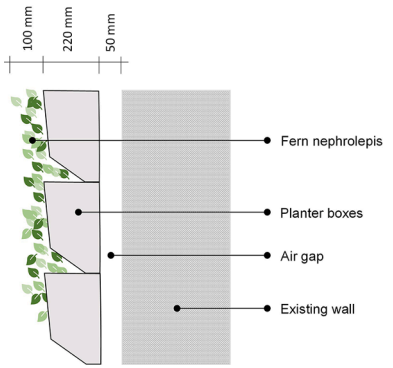

Layers	Materials	Thickness [mm]	CO_2 fixation mode	Leaf type	Albedo	Transmittance	Leaf area density [a]	Root area density [b]	LAI	Root Zone Depth	Season profile
Vegetation	Mix of sedum [c]	200	C3	Deciduous	0.11	0.3	0.15	0.1	3	0.5	1
Vegetation	Hedera helix [c]	100	C3	Deciduous	0.2	0.3	0.15	0.1	3	0.5	1
Vegetation	Fern Nephrolepis [c]	100	C3	Deciduous	0.2	0.3	0.15	0.1	3.79 [d]	0.5	1
			Water content at saturation [m^3/m^3]	**Water content at field capacity [m^3/m^3]**	**Water content at wilting point [m^3/m^3]**	**Matrix potential [m]**	**Hydraulic conductivity [m/s * 10^{-6}]**	**Volumetric heat capacity [J/m^3K*10^{-6}]**	**Clapp and Hornberger's b constant**	**Thermal conductivity [W/mK]**	
Growing medium [e]	Lapillus 54.6% Pumice 21% Peat 16% Zeolite 8.4%	100	0.4[f]	0.18646[g]	0.16500[f]	−0.09000[h]	800[f]	1.32840 [i]	438.000[h]	0.33000 [i]	
Filter membrane	Polypropylene	1	0	0	0	0	0	0.05231	0	0.04900	
Drainage layer	Polystyrene foam in grains	50									
Waterproofing barrier	Bitumen	10	0	0	0	0	0	120.000	0	0.17000	

3.3.1. Turin

For the simulated area in Turin, it has been found that all three mitigation scenarios produce a negligible average daily reduction in the air temperature (i.e., 0.02 °C) at the pedestrian level for the typical winter day (Table 6 lines 2–4).

Table 6 displays that, at 10.00 am (i.e., when both the TO1 and the TO2 scenarios exert the greatest UHI mitigation), TO1 and TO2 scenarios have similar effects on average air temperature reduction over either the whole simulated area (i.e., about 0.05 °C) or within the canyon (i.e., about 0.1 °C); and these latter are both negligible. Besides, at 07.00 am, the average UHI mitigation effect of the TO3 scenario in the whole area is negligible (i.e., 0.03 °C), but local mitigation effects within the canyon can be as high as 0.36 °C (Fig. 3).

For the typical summer day, Table 6 shows that, for the whole urban area, the average daily decrease in air temperature is negligible (i.e., between 0.01 °C and 0.03 °C) for all the scenarios; nevertheless, in the hour of maximum mitigation, the greatest decrease in air temperature varies from 0.29 °C to 0.56 °C locally. Specifically, Figs. 4-6 exhibit that: for all three scenarios, the mitigation effect is localized only within the canyon; there are no differences between the UHI mitigation exerted by LWs (i.e., TO1) and GFs (i.e., TO2) in a canyon parallel to the wind direction (i.e., the average mitigation within the canyon equals 0.26 °C, and the maximum local mitigation is as high as 0.56 °C); the application of LWs in a canyon orthogonal to the wind direction (i.e., TO3) exerts a mitigation effect only in the central part of the canyon equal to 0.29 °C.

The mitigation effect of the three scenarios has also been evaluated considering the typical heat wave day. Table 6 shows that likewise for the typical summer day, for the whole urban area, the average daily decrease in air temperature exerted by each scenario is negligible (i.e., from 0.01 °C to 0.04 °C). Nevertheless, Figs. 7, 8 showcase that the mitigation effect exerted by the TO1 and TO2 scenarios is limited to the canyons where the BIVTs are applied. Moreover, LWs and GFs applied in a canyon parallel to the wind direction reduce the average air temperature within the canyon by approximately 0.22 °C with local peaks of about 0.5 °C. Contrariwise, LWs are ineffective in mitigating UHI when applied in a canyon orthogonal to the wind direction (i.e., TO3 scenario) since the maximum local peak mitigation value is negligible (i.e., 0.13 °C).

3.3.2. Rome

For the selected urban area in Rome, it has been found that for the typical winter day, the three mitigation scenarios exert a negligible average daily decrease in urban overheating (Table 6, lines 5–7). Besides, the greatest decrease (i.e., 0.33 °C) in the average air mitigation on the whole area is achieved at 01.00 am when scenario RM2, which implements both EGRs and GFs, is applied (Table 6 line 12). Contrariwise, the application of the other two scenarios entails negligible average air mitigation (Table 6, lines 11–13).

Fig. 9 displays that the greatest air temperature decrease, due to the application of scenario RM2 and equal to approximately 0.8 °C, is confined to the central part of the urban area and in narrow streets and courtyards where the cooled air is trapped. Contrariwise, in wider streets, such as in the North part of the area, the air mitigation ranges from approximately 0.1 to 0.4 °C.

The analyses of the summer mitigation potentials of the three scenarios (Table 6, lines 5–7) show that the daily average temperature variations are all negligible.

As far as the hours of the day showing the greatest mitigation potential (i.e., 03.00 pm for scenarios RM1 and RM2, and 05.00 pm for scenario RM3) are concerned (Table 6 lines 11–13), the average UHI reduction is negligible for the RM1 and RM3 scenarios, but for scenario RM2 it equals 0.33 °C. Furthermore, locally, scenarios RM1 and RM2 show a maximum decrease in air temperature equal to 0.36 °C and 1.17 °C, respectively. Specifically, Fig. 10 shows that the RM1 scenario decreases air temperature up to approximately 0.36 °C in the southern-eastern part of the urban area due to the wind direction. Furthermore, the EGR installation decreases to the greatest extent the pedestrian air temperature within courtyards where wind conveys cooled air. Differently, the effect of EGR installation is negligible in the other zones of the urban area, such as the western part.

For scenario RM2, Fig. 11 displays that in most of the investigated urban area, the decrease in air temperature equals 0.7–0.8 °C with peaks of 1.17 °C within courtyards. Furthermore, it can be noticed that the UHI mitigation extent depends on both wind direction and street width. Specifically, the greatest UHI mitigation is reached in downwind narrow streets, and the UHI mitigation potential decreases in wide streets (i.e., in the northern part of the urban area). Compared to scenario RM1, scenario RM2 shows the greatest decrease in local air temperature, revealing that GFs are more beneficial than EGRs in decreasing air temperature for the present case study.

The effect of the mitigation scenarios has also been investigated on a typical summer day with a heat wave. Table 6 (lines 5–7) shows that the daily average decreases in air temperature due to the application of the three mitigation scenarios are negligible.

Furthermore, it can be observed that during the hours of maximum mitigation (i.e., 05.00 pm), the average UHI reduction is negligible for scenarios RM1 and RM3 and is equal to 0.35 °C when the RM2 scenario is applied.

The greatest local air temperature variations have been discussed in the following when significant. Specifically, Fig. 12 showcases that, applying the RM1 scenario, the greatest UHI mitigation (i.e., approximately 0.3 °C) is reached in a courtyard, where, because of wind direction, the cooled air is trapped by buildings.

Scenario RM2 decreases air temperature up to approximately 0.9 °C compared to the reference scenario (Fig. 13). Such a decrease regards most of the investigated urban area; however, in the proximity of wide streets (i.e., in the northern part of the map), the UHI mitigation is restricted to about 0.4 °C the most. In the proximity of narrow streets, the UHI mitigation exceeds 0.8 °C. The distribution of the isotherms of the UHI mitigation largely depends on wind direction.

4. Discussion

Unlike most published literature, which mainly reports on the mitigation potential of BIVTs referred only to a specific test point [65], the present study also presents spatially averaged UHI mitigation values. These latter values can support decision makers, who design policies to reduce urban overheating better than test points since they refer to wider areas. Furthermore, the present study investigates UHI and UHI mitigation potential BIVT-based scenarios in winter, summer, and summer with heat wave typical days. Lastly, the article shows the results of modeling two urban areas characterized by two different urban patterns, expanding the questions about the effect of applying BIVT-based mitigation scenarios and making the investigation results generalizable.

To test the study's solidity, we first compared the measured UHI magnitude for the two urban areas with the values found in the literature. In Turin, the average UHI for the typical winter and summer days equals 2.4 °C and 1.1 °C with a peak of 4.4 °C in the early morning hours, respectively, in accordance with the values found by Milelli [66]. For the selected urban area in Rome, and in accordance with Battista et al. [67] and Zinzi et al. [68], the winter UHI equals 0.4 °C with peaks of 1.5 °C, and the summer UHI equals 2.2 °C with peaks of 2.9–3.8 °C. The UHI magnitude of the typical summer days with a heat wave are innovative since, so far, no studies investigated such an aspect.

Albeit the analysis of published literature shows that the number of studies exploring the effect of green walls on winter air temperature is very exiguous [69,70], we found that, in accordance with the findings provided by Wong et al. [71], for both urban areas (i.e., Turin and Rome) the average winter temperature decrease is negligible considering all the proposed scenarios except the RM2 (Table 6 lines 8–13). For both case studies, the mitigation scenarios' ineffectiveness is due to the limited plants' biological activity and incoming solar radiation in winter

Fig. 2. Scenarios applied to the selected urban areas.

Table 5
MAE, RMSE values for the case studies of Turin and Rome (lines 1–7). Comparison between the calculated values and the values found in the literature (box and whiskers charts. Data modified from Tsoka et al. [63]. Red and black dots represent MAE and RMSE values for the case studies of Rome and Turin, respectively.

	Typical days	Mean Absolute Error (MAE)	Root Mean Square Error (RMSE)
Turin	Winter	1.91 °C	2.08 °C
	Summer	1.06 °C	1.37 °C
	Heat wave	1.22 °C	1.47 °C
Rome	Winter	0.38 °C	0.52 °C
	Summer	1.89 °C	2.02 °C
	Heat wave	1.60 °C	1.95 °C

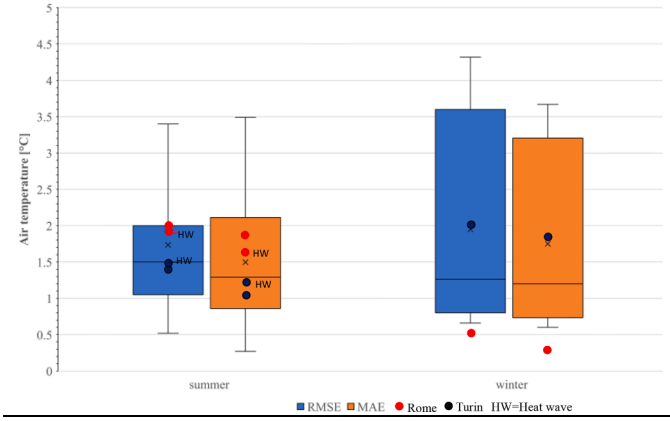

[32,72]. Furthermore, for scenario RM1, the inefficacy in decreasing winter UHI is also due to the building height where EGRs are installed since EGR effectiveness decreases with the increase in the building height [31,73]. Jin et al. [74] found that EGRs have the greatest UHI mitigation potential when installed on 10 m high buildings; besides, applying EGRs on 40 m high buildings has null effect [74,75].

Furthermore, another distinctive factor in mitigating UHI is the BIVTs' application scale. The comparison of the mitigation effects of the applied scenarios shows that the higher the amount of BIVTs installed, the greater the UHI mitigation. For example, scenario RM2 shows a maximum decrease in air temperature averaged on the whole area of 0.35 °C and a maximum punctual reduction of 0.84 °C. Comparing such a result with the mitigation effect of scenario RM3 and in agreement with previous studies [76,77], it results that the scale factor is crucial in reducing UHI. This effect is also amplified by the fact that scenario RM2 includes EGR and GF installation. EGRs show a decreasing mitigation with the increase in the building height resulting inefficient in mitigating UHI, and GFs show a rising mitigation potential with the increase

Table 6
Results of the application of the UHI mitigation scenarios.

	Typical winter day[a,b]	Typical summer day[c,d]	Typical summer day with a heat wave[e,f]
Average daily UHI mitigation [°C] TO1	−0.02	−0.03	−0.04
Average daily UHI mitigation [°C] TO2	−0.02	−0.03	−0.04
Average daily UHI mitigation [°C] TO3	−0.02	−0.01	−0.01
Average daily UHI mitigation [°C] RM1	0.00	−0.04	−0.04
Average daily UHI mitigation [°C] RM2	−0.18	−0.22	−0.21
Average daily UHI mitigation [°C] RM3	0.00	−0.01	−0.01
TO1 Avg (Max; min) mitigation [°C]*	−0.05 (-0.18; 0.02) [g]	−0.10 (-0.56; 0.02) [h]	−0.10 (-0.46; −0.01) [h]
TO2 Avg (Max; min) mitigation [°C]*	−0.05 (-0.18; 0.02) [g]	−0.09 (-0.54; 0.02) [h]	−0.08 (-0.48; −0.01) [i]
TO3 Avg (Max; min) mitigation [°C]*	−0.03 (-0.36; 0.01) [j]	−0.02 (-0.29; 0.01) [k]	−0.03 (-0.13; 0.00) [h]
RM1 Avg (Max; min) mitigation [°C]*	−0.01 (-0.10; 0.02) [l]	−0.08 (-0.36; 0.22) [m]	−0.06 (-0.25; 0.00) [h]
RM2 Avg (Max; min) mitigation [°C]*	−0.35 (-0.84; 0.01) [l]	−0.33 (-1.17; 0.13) [m]	−0.35 (-0.92; 0.00) [h]
RM3 Avg (Max; min) mitigation [°C]*	0.00 (-0.20; 0.00) [l]	−0.01 (-0.07; 0.23) [m]	−0.01 (-0.13; 0.00) [h]

[a] Turin typical winter day: 19/01/2016
[b] Rome typical winter day: 19/02/2015
[c] Turin typical summer day: 27/07/2014
[d] Rome typical summer day: 01/07/2015
[e] Turin typical summer day with a heat wave: 07/07/2015
[f] Rome typical summer day with a heat wave: 22/07/2015
[g] Temperature mitigation hour: 10:00 am
[h] Temperature mitigation hour: 05:00 pm
[i] Temperature mitigation hour: 06:00 pm
[j] Temperature mitigation hour: 07:00 am
[k] Temperature mitigation hour: 07:00 pm
[l] Temperature mitigation hour: 01:00 am
[m] Temperature mitigation hour: 03:00 pm
* Spatially averaged

of the building height where they are installed [71,75,77,78]. In accordance with previous research (i.e., [31], Fig. 10 shows that the greatest air temperature decrease entailed by scenario RM2 (i.e., 0.84 °C) is confined to the central part of the urban area where narrow streets and courtyards trap the cooled air.

The analyses of the results of the summer simulations of the two urban areas show that all the scenarios exert a negligible average summer UHI mitigation (Table 6, lines 8–13) except scenario RM2. Specifically, scenario RM2 showcases a maximum decrease in air temperature averaged on the selected urban area equal to 0.33 °C. Furthermore, by comparing the average mitigation potential of scenarios RM1 and RM2 (Table 6, lines 11–12), which are featured by the same scale of application but different BIVTs, it results that, for the examined urban pattern, GF installation is more beneficial than EGRs. Such findings are consistent with those provided by Iaria & Susca [72], who found that EGRs are inefficient in mitigating urban overheating when installed on 20 m-tall buildings; contrariwise, the mitigation effect of GFs increases with the increase in building height on which they are installed.

Moreover, all the scenarios, except scenario RM3, show significant maximum local decreases in air temperature. Specifically, in Turin, in accordance with previous research by Alexandri & Jones [79], the application of LWs in a canyon orthogonal to the wind direction (i.e., TO3) is less effective than the one in a canyon parallel to the wind (i.e., TO1): the maximum and the average mitigation values within the canyons are equal to 0.29 °C and 0.16 °C when scenario TO3 is applied, and to 0.56 °C and 0.26 °C when scenario TO1 is applied. Besides, applying LWs or GFs (i.e., scenarios TO1 and TO2, respectively) do not show any significant modification in UHI mitigation (Table 6 lines 8–9), revealing that the wind direction is a predominant factor compared to the BIVT typology.

As the UHI mitigation in Rome is concerned, comparing the local average UHI mitigation values related to the application of scenario RM1 and RM2 results in GFs being more beneficial than EGRs in decreasing air temperature. Such a result is mainly attributable to the height of the buildings where the two BIVTs are applied (i.e., the average building height is equal to approximately 20 m). Such a result is confirmed by the findings of previous research (i.e., [71], which shows that the effectiveness of EGR and GF installation in mitigating air temperature is respectively indirectly and directly correlated to the height of

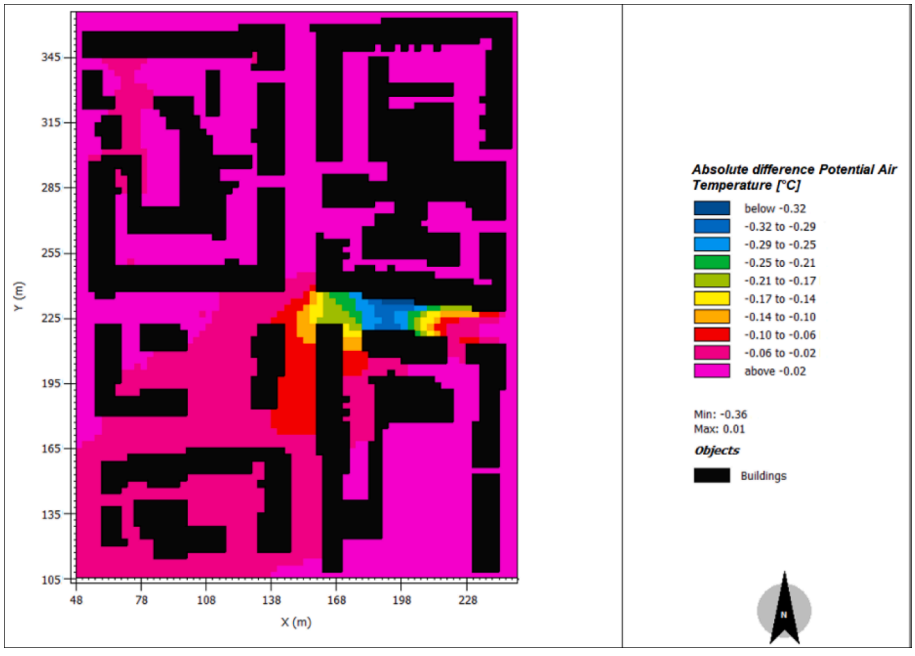

Fig. 3. Comparison between TO3 scenario and baseline one air temperature at pedestrian level (i.e., 2.1 m above the ground) at 07.00 am for the typical winter day (i.e., 19/01/2016).

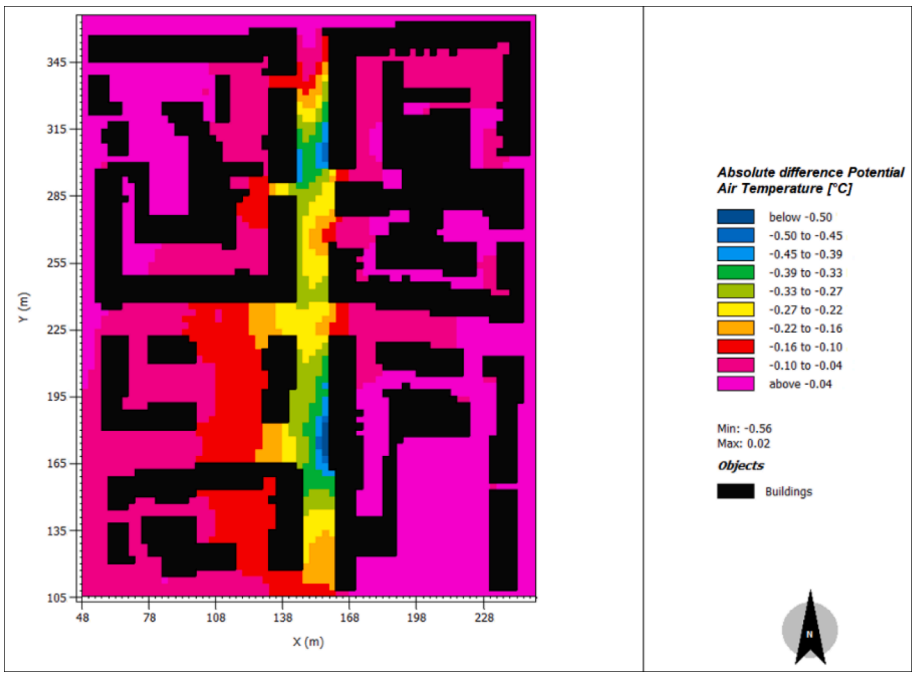

Fig. 4. Comparison between TO1 scenario and baseline one air temperature at pedestrian level (i.e., 2.1 m above the ground) at 05.00 pm for the typical summer day (i.e., 27/07/2014).

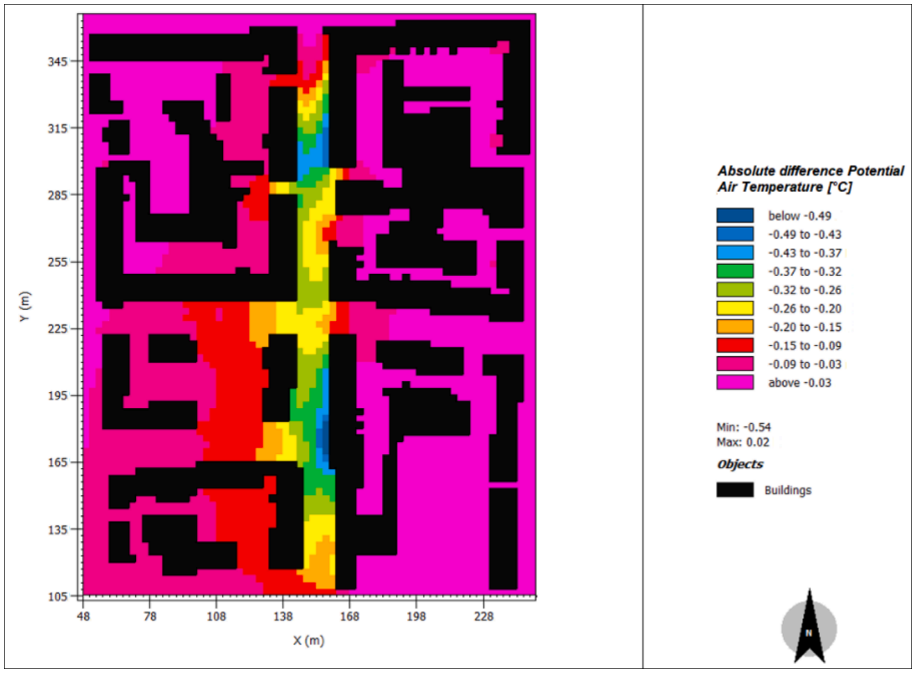

Fig. 5. Comparison between TO2 scenario and baseline one air temperature at pedestrian level (i.e., 2.1 m above the ground) at 05.00 pm for the typical summer day (i.e., 27/07/2014).

the buildings where the BIVTs are installed. Fig. 11 shows that the RM1 scenario at 03.00 pm decreases air temperature up to approximately 0.36 °C in the courtyards in the southern-eastern part of the urban area where the cooled air is trapped due to the wind direction. This finding is consistent with the decrease in air temperature related to the application of GRs in the Yangtze River Delta urban agglomeration [80]. Besides, the application of the RM3 scenario produces a null thermal effect on the UHI, which confirms the importance of the scale of application of BIVTs for their UHI mitigation potential.

Innovatively, the mitigation effect of the three scenarios has also been evaluated considering the typical heat wave day since, to the authors' best knowledge, no studies about heat wave temperature mitigation can be found in the literature, although they are becoming more frequent extreme climate phenomena [81]. By analyzing the simulation outputs, it results that, except for the application of scenario RM2, with the increase in air temperature, the average mitigation performance of the BIVT-based scenarios on the whole area remains negligible (Table 6 lines 8–10). Such a finding is in accordance with that found by Gromke

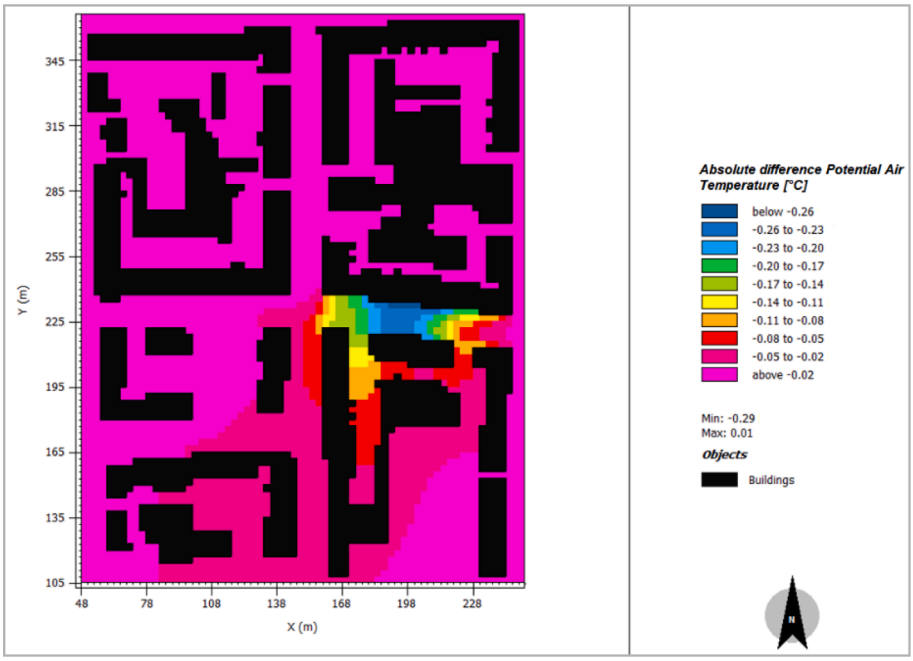

Fig. 6. Comparison between TO3 scenario and baseline one air temperature at pedestrian level (i.e., 2.1 m above the ground) at 07.00 pm for the typical summer day (i.e., 27/07/2014).

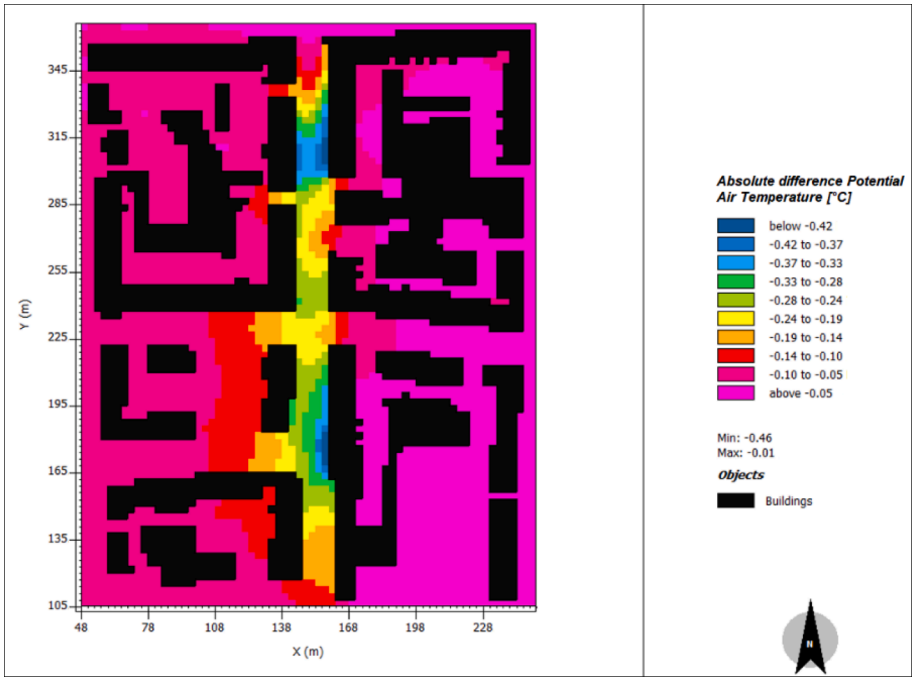

Fig. 7. Comparison between TO1 scenario and baseline one air temperature at pedestrian level (i.e., 2.1 m above the ground) at 05.00 pm for the typical summer day with a heat wave (i.e., 07/07/2015).

et al. [82], and the reason is twofold: 1. all the scenarios, except scenarios RM1 and RM2, are related to the application of BIVTs to a limited part of the simulated built environment; 2. scenario RM1 entails the large scale application of EGRs, which show very limited effectiveness in mitigating UHI when applied to high-rise buildings. Contrariwise, the broad application of GFs (i.e., scenario RM2) shows a maximum average decrease in air temperature equal to 0.35 °C. Moreover, as for the summer day, in Turin, for the summer day with a heat wave, the application of LWs in a canyon orthogonal to the wind direction (i.e., TO3) is less effective than the one in a canyon parallel to the wind (i.e., TO1).

By the comparison of the simulation outputs related to the application of the three mitigation scenarios to the selected urban area in Rome, it results that the average decrease in UHI is negligible when scenarios RM1 and RM3 are applied; contrariwise, the application of scenario RM2 entails an average UHI mitigation for the whole urban area equal to 0.35 °C. Furthermore, comparing the mitigation potentials of the three scenarios with those related to the typical summer day results in the average mitigation values being approximately equal (Table 6, lines 11–13). Moreover, as far as the maximum decrease in air temperature is

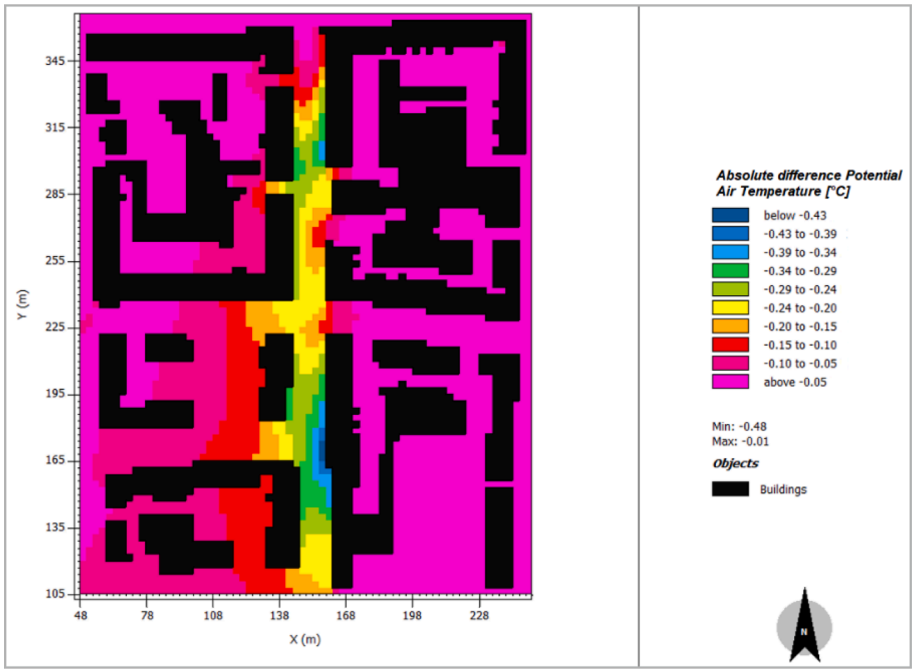

Fig. 8. Comparison between TO2 scenario and baseline one air temperature at pedestrian level (i.e., 2.1 m above the ground) at 06.00 pm for the typical summer day with a heat wave (i.e., 07/07/2015).

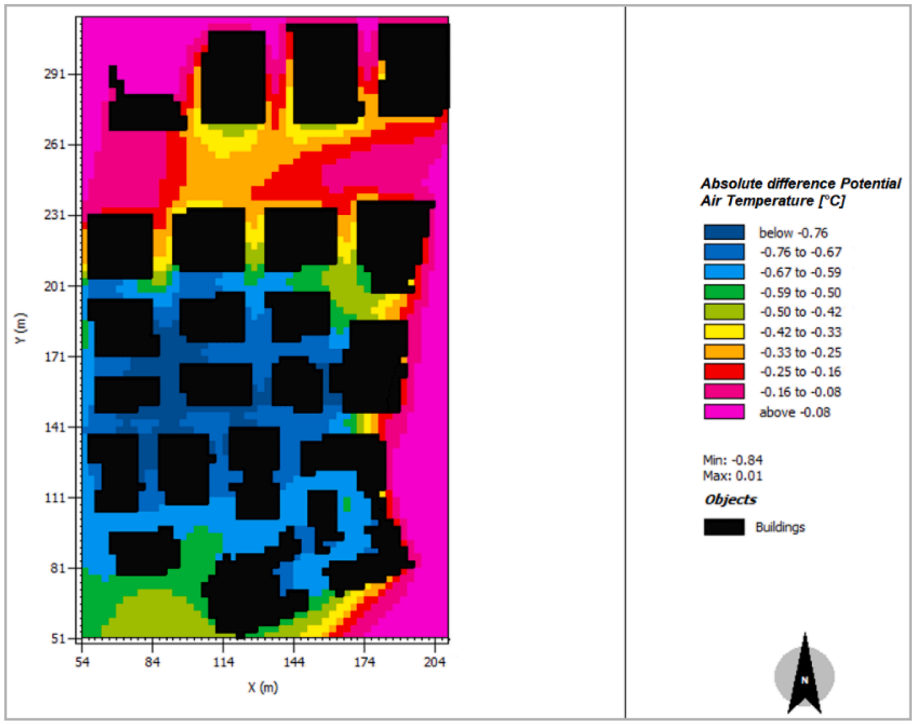

Fig. 9. Comparison between RM2 scenario and baseline one air temperature at pedestrian level (i.e., 2.1 m above the ground) at 01.00 am for the typical winter day (i.e., 19/02/2015).

concerned, the application of the RM2 scenario exerts the greatest local mitigation potential, confirming the importance of the application scale of the mitigation scenario and the effectiveness of GFs compared to EGRs. Lastly, we found that in most cases, the local maximum temperature mitigation is lower than that related to the typical summer day because of the modified biological activity of plants caused by heat stress [83,84]. This finding is in accordance with J. Zhao et al. [85], which shows that heat waves decrease the cooling potential of plants in Mediterranean cities due to large stomatal closures.

5. Conclusions

The proposed study investigates the effect of the BIVTs on mitigating UHI in the Italian cities: Turin and Rome. ENVI-met software has been used to model two built areas within the two cities and to simulate the microclimate effect of three UHI mitigation scenarios for each area. The

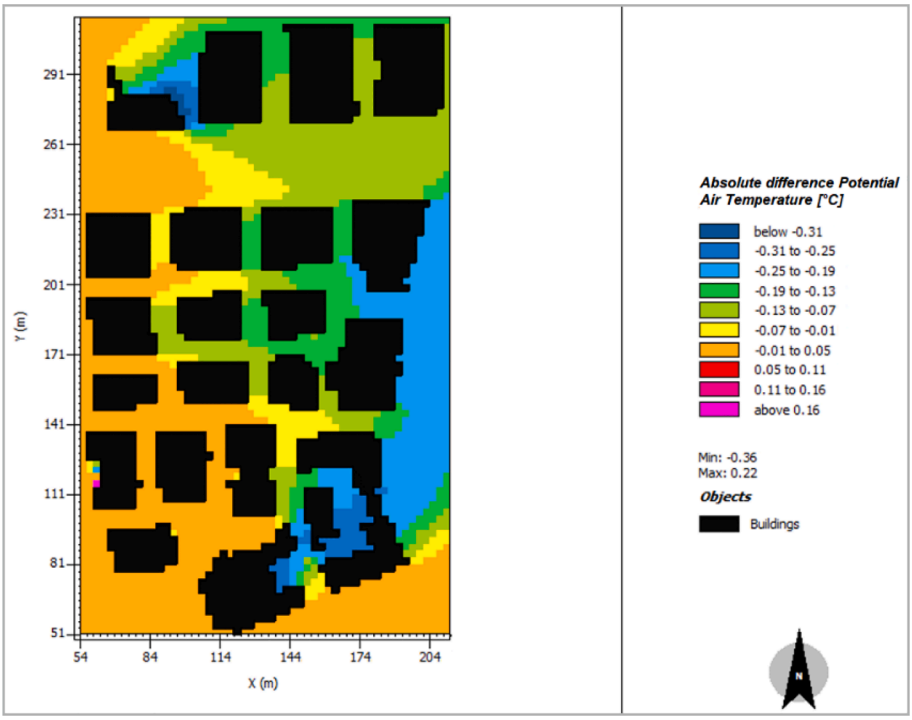

Fig. 10. Comparison between RM1 scenario and baseline one air temperature at pedestrian level (i.e., 2.1 m above the ground) at 03.00 pm for the typical summer day (i.e., 01/07/2015).

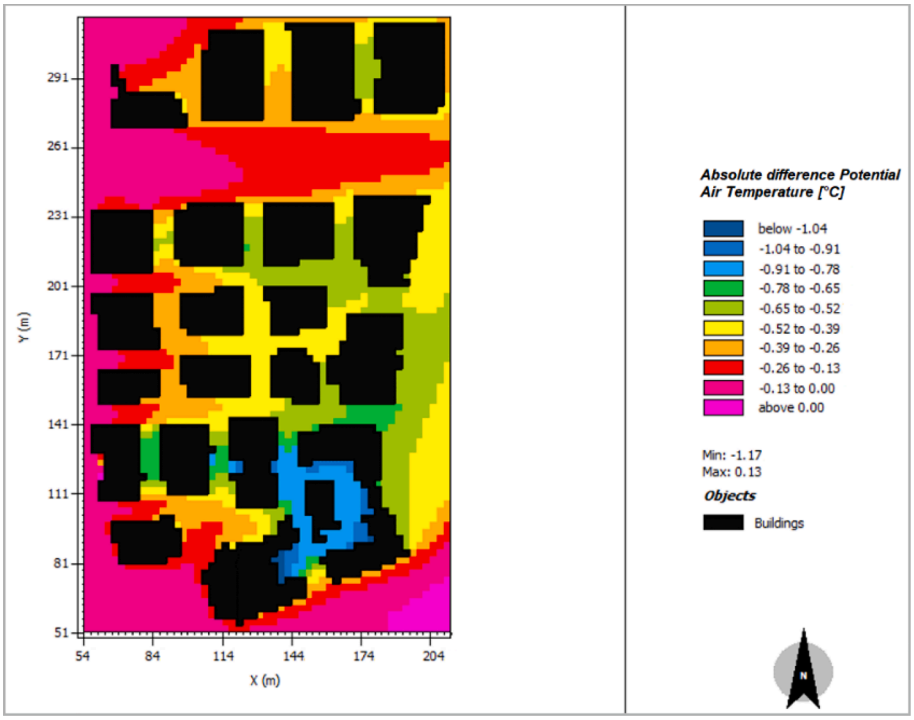

Fig. 11. Comparison between RM2 scenario and baseline one air temperature at pedestrian level (i.e., 2.1 m above the ground) at 03.00 pm for the typical summer day (i.e., 01/07/2015).

application of the developed scenarios to the two built areas has been simulated for a typical winter day, a typical summer day, and a typical summer day with a heat wave.

The results of the simulations have shown the importance of the scale of application of the UHI mitigation strategies. Specifically, when GFs are applied to a single building (i.e., scenario RM3), their air temperature mitigation potential is negligible; contrariwise, a broad application of UHI mitigation strategies may provide a greater decrease in urban warming (i.e., scenario RM2). Furthermore, the simulation results show that EGRs and green walls generally decrease to a more limited extent air temperature in winter than in summer, likely due to the limited biological activity of plants.

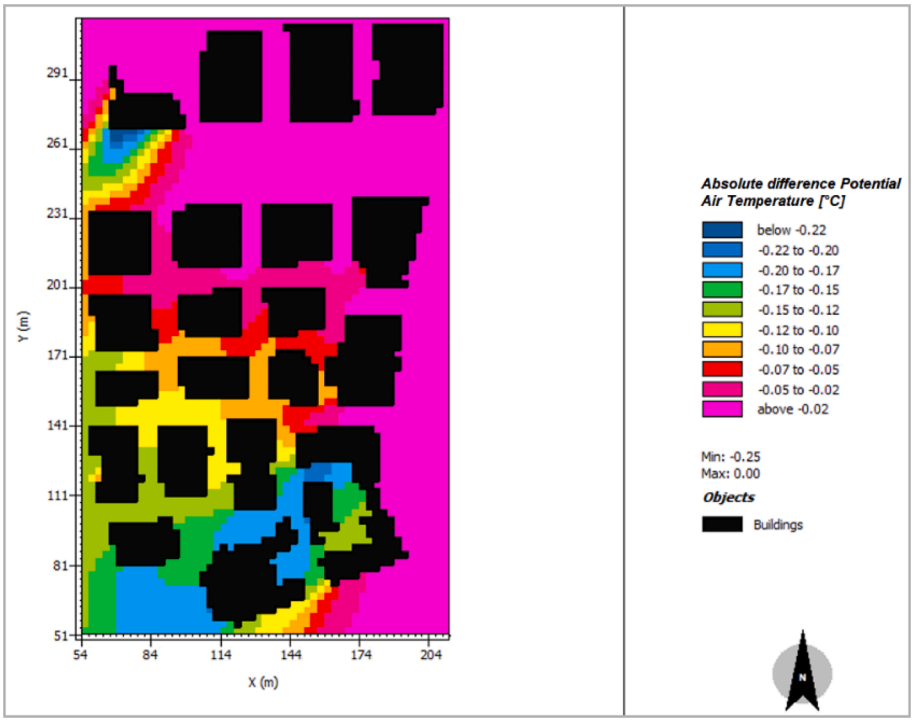

Fig. 12. Comparison between RM1 scenario and baseline one air temperature at pedestrian level (i.e., 2.1 m above the ground) at 05.00 pm for the typical summer day with a heat wave (i.e., 22/07/2015).

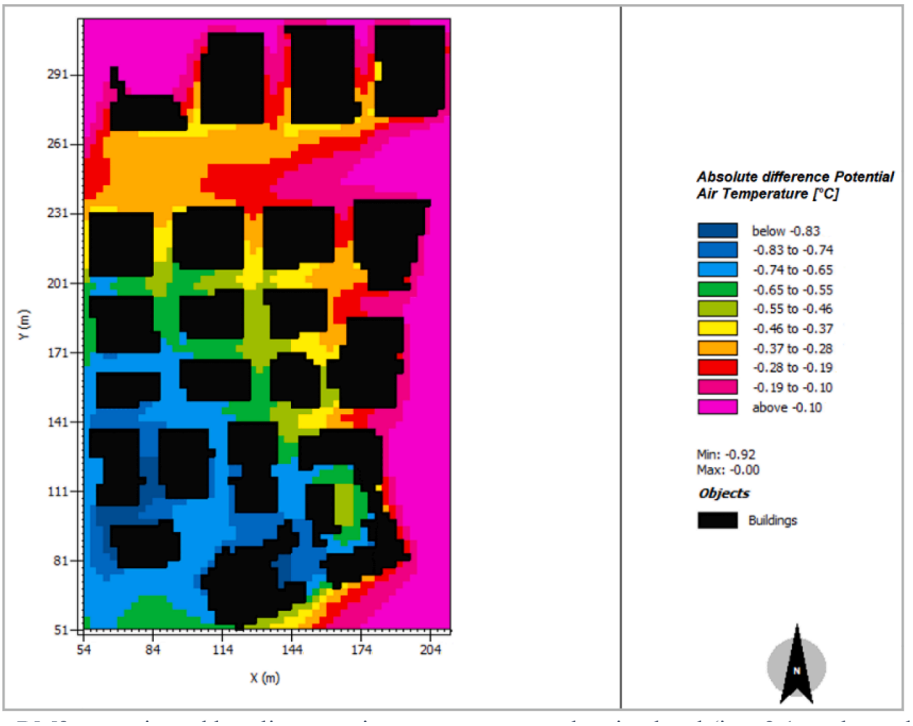

Fig. 13. Comparison between RM2 scenario and baseline one air temperature at pedestrian level (i.e., 2.1 m above the ground) at 05.00 pm for the typical summer day with a heat wave (i.e., 22/07/2015).

The UHI mitigation potential of the different scenarios may depend on the urban areas' geometry. Although none of the developed scenarios can nullify the UHI in Rome, GFs (i.e., scenario RM2) decrease urban temperatures up to about 1.2 °C, considerably alleviating urban temperatures. Contrariwise, the geometrical features of the analyzed area in Turin allow a more limited decrease in urban temperature up to about 0.6 °C (i.e., TO1 and TO2 scenarios).

The study results also provide a guide for urban policymakers offering a relative measure of BIVT-based urban mitigation scenarios' effectiveness. For instance, in a densely urbanized area characterized by high-rising buildings, green walls are more beneficial in mitigating UHI than EGRs, which have a negligible effect on urban warming (i.e.,

scenario RM2 vs. RM1). Furthermore, the Turin case study shows that BIVTs are more effective in mitigating summer UHI when installed in canyons parallel to the main wind direction than in perpendicular ones, and it shows that it is necessary to increase plant watering to promote the stomatal opening for adapting to UHI during summer heat waves.

All in all, when policymakers aim at urban adaptation, they should impose wide deployment of BIVTs favoring GFs when tall buildings feature urban areas; contrariwise, the deployment of EGRs can be more beneficial in reducing building energy use [32], and, consequently, heat waste from cooling systems which indirectly reduce summer overheating [86]. When BIVTs cannot be extensively installed, albeit local decreases can be achieved in urban temperature, they should be coupled with other mitigation measures to reduce UHI efficiently. In this context, United Nations has supported the whole system approach to beat urban overheating, which relies on the simultaneous application of various mitigation measures [87,88].

Funding

This work was supported by MiTE (Italian Ministry for the Ecological Transition) [Fondo per il finanziamento delle attività di ricerca e di sviluppo di interesse generale per il sistema elettrico nazionale].

CRediT authorship contribution statement

Tiziana Susca: Conceptualization, Methodology, Validation, Formal analysis, Investigation, Resources, Writing – original draft, Writing – review & editing, Visualization, Supervision. **Fabio Zanghirella:** Conceptualization, Methodology, Validation, Formal analysis, Investigation, Writing – original draft, Writing – review & editing, Visualization, Supervision. **Vincenzo del Fatto:** Data curation, Writing – original draft, Writing – review & editing, Visualization, Resources.

Declaration of Competing Interest

The authors declare the following financial interests/personal relationships which may be considered as potential competing interests: Tiziana Susca, Fabio Zanghirella, Vincenzo Del Fatto report financial support was provided by Government of Italy Ministry of Ecological Transition.

Data availability

All the necessary data have been shown in the appendices

Appendix A. Supplementary data

Supplementary data to this article can be found online at https://doi.org/10.1016/j.enbuild.2023.113233.

References

[1] Ritchie, H., & Roser, M. (2013). *Land Use*. OurWorldInData.org. https://ourworldindata.org/land-use.
[2] The World Bank, Urban population | Data, The World Bank. (2018). https://data.worldbank.org/indicator/SP.URB.TOTL.IN.ZS.
[3] United Nations. (2018). World Urbanization Prospects—Population Division—United Nations (2018). https://population.un.org/wup/Download/.
[4] T.R. Oke, The energetic basis of the urban heat island, Q. J. R. Meteorolog. Soc. 108 (455) (1982) 1–24, https://doi.org/10.1002/qj.49710845502.
[5] Zhou, D., Xiao, J., Frolking, S., Zhang, L., & Zhou, G. (2022). Urbanization Contributes Little to Global Warming but Substantially Intensifies Local and Regional Land Surface Warming. *Earth's Future*, *10*(5), e2021EF002401. 10.1029/2021EF002401.
[6] P. Fu, Q. Weng, Variability in annual temperature cycle in the urban areas of the United States as revealed by MODIS imagery, ISPRS J. Photogramm. Remote Sens. 146 (2018) 65–73, https://doi.org/10.1016/j.isprsjprs.2018.09.003.
[7] D.A. Hartz, L. Prashad, B.C. Hedquist, J. Golden, A.J. Brazel, Linking satellite images and hand-held infrared thermography to observed neighborhood climate conditions, Remote Sens. Environ. 104 (2) (2006) 190–200, https://doi.org/10.1016/j.rse.2005.12.019.
[8] Y.-R. Wang, D.O. Hessen, B.H. Samset, F. Stordal, Evaluating global and regional land warming trends in the past decades with both MODIS and ERA5-Land land surface temperature data, Remote Sens. Environ. 280 (2022), 113181, https://doi.org/10.1016/j.rse.2022.113181.
[9] C. Yang, F. Yan, S. Zhang, Comparison of land surface and air temperatures for quantifying summer and winter urban heat island in a snow climate city, J. Environ. Manage. 265 (2020), 110563, https://doi.org/10.1016/j.jenvman.2020.110563.
[10] R.D.S. Cardoso, L.P. Dorigon, D.C.F. Teixeira, M.C. de Amorim, C. t., Assessment of Urban Heat Islands in Small- and Mid-Sized Cities in Brazil, Climate 5 (1) (2017) Art. 1, https://doi.org/10.3390/cli5010014.
[11] D.K. Papanastasiou, C. Kittas, Maximum urban heat island intensity in a medium-sized coastal Mediterranean city, Theor. Appl. Climatol. 107 (3) (2012) 407–416, https://doi.org/10.1007/s00704-011-0491-z.
[12] B. Zhou, D. Rybski, J.P. Kropp, The role of city size and urban form in the surface urban heat island, Sci. Rep. 7 (1) (2017) Art. 1, https://doi.org/10.1038/s41598-017-04242-2.
[13] K. Lee, Y. Kim, H.C. Sung, J. Ryu, S.W. Jeon, Trend Analysis of Urban Heat Island Intensity According to Urban Area Change in Asian Mega Cities, Sustainability 12 (1) (2020) Art. 1, https://doi.org/10.3390/su12010112.
[14] M. Santamouris, On the energy impact of urban heat island and global warming on buildings, Energ. Buildings 82 (2014) 100–113, https://doi.org/10.1016/j.enbuild.2014.07.022.
[15] M. Santamouris, C. Cartalis, A. Synnefa, D. Kolokotsa, On the impact of urban heat island and global warming on the power demand and electricity consumption of buildings—A review, Energ. Buildings 98 (2015) 119–124, https://doi.org/10.1016/j.enbuild.2014.09.052.
[16] G. Ulpiani, On the linkage between urban heat island and urban pollution island: Three-decade literature review towards a conceptual framework, Sci. Total Environ. 751 (2021), 141727, https://doi.org/10.1016/j.scitotenv.2020.141727.
[17] C. Heaviside, H. Macintyre, S. Vardoulakis, The Urban Heat Island: Implications for Health in a Changing Environment, Current Environmental Health Reports 4 (3) (2017) 296–305, https://doi.org/10.1007/s40572-017-0150-3.
[18] United Nations. (2015). *THE 17 GOALS | Sustainable Development*. United Nations - Department of Economic and Social Affairs Sustainable Development. https://sdgs.un.org/goals.
[19] H. Farhadi, M. Faizi, H. Sanaieian, Mitigating the urban heat island in a residential area in Tehran: Investigating the role of vegetation, materials, and orientation of buildings, Sustain. Cities Soc. 46 (2019), 101448, https://doi.org/10.1016/j.scs.2019.101448.
[20] A. Price, E.C. Jones, F. Jefferson, Vertical Greenery Systems as a Strategy in Urban Heat Island Mitigation, Water Air Soil Pollut. 226 (8) (2015) 247, https://doi.org/10.1007/s11270-015-2464-9.
[21] W.D. Solecki, C. Rosenzweig, L. Parshall, G. Pope, M. Clark, J. Cox, M. Wiencke, Mitigation of the heat island effect in urban New Jersey, Global Environ. Change B. Environ. Hazard 6 (1) (2005) 39–49, https://doi.org/10.1016/j.hazards.2004.12.002.
[22] T. Susca, S.R. Gaffin, G.R. Dell'Osso, Positive effects of vegetation: Urban heat island and green roofs, Environ. Pollut. 159 (8) (2011) 2119–2126, https://doi.org/10.1016/j.envpol.2011.03.007.
[23] T. Susca, Nature-based-solutions applied to the built environment to alleviate climate change, Maximilian Lackner, Baharak Sajjadi, Wei-Yin Chen, In Handbook of Climate Change Mitigation and Adaptation (Springer Nature), 2022.
[24] T. Safikhani, A.M. Abdullah, D.R. Ossen, M. Baharvand, A review of energy characteristic of vertical greenery systems, Renew. Sustain. Energy Rev. 40 (2014) 450–462, https://doi.org/10.1016/j.rser.2014.07.166.
[25] M. Manso, J. Castro-Gomes, Green wall systems: A review of their characteristics, Renew. Sustain. Energy Rev. 41 (2015) 863–871, https://doi.org/10.1016/j.rser.2014.07.203.
[26] G. Pérez, J. Coma, Chapter 2.3—Green Roofs Classifications, Plant Species, Substrates, in: G. Pérez, K. Perini (Eds.), Nature Based Strategies for Urban and Building Sustainability, Butterworth-Heinemann, 2018, pp. 65–74, https://doi.org/10.1016/B978-0-12-812150-4.00006-9.
[27] J.R. Simpson, Improved estimates of tree-shade effects on residential energy use, Energ. Buildings 34 (10) (2002) 1067–1076.
[28] N.H. Wong, C.L. Tan, D.D. Kolokotsa, H. Takebayashi, Greenery as a mitigation and adaptation strategy to urban heat, Nature Reviews Earth & Environment 2 (3) (2021) 166–181, https://doi.org/10.1038/s43017-020-00129-5.
[29] Oke, T. R. (2009). *Boundary layer climates*. https://login.lacollegelibrary.idm.oclc.org/login?url=http://search.ebscohost.com/login.aspx?direct=true&scope=site&db=nlebk&AN=74015.
[30] K. Vijayaraghavan, Green roofs: A critical review on the role of components, benefits, limitations and trends, Renew. Sustain. Energy Rev. 57 (2016) 740–752, https://doi.org/10.1016/j.rser.2015.12.119.
[31] T. Susca, Green roofs to reduce building energy use? A review on key structural factors of green roofs and their effects on urban climate, Build. Environ. 162 (2019), 106273, https://doi.org/10.1016/j.buildenv.2019.106273.
[32] T. Susca, F. Zanghirella, L. Colasuonno, V. Del Fatto, Effect of green wall installation on urban heat island and building energy use: A climate-informed systematic literature review, Renew. Sustain. Energy Rev. 159 (2022), 112100, https://doi.org/10.1016/j.rser.2022.112100.
[33] G. Evola, F. Nocera, V. Costanzo, M. Detommaso, S. Bonaccorso, L. Marletta, Greenery Systems for the Mitigation of the Urban Heat Island: A Simulation Experience for Southern Italy, in: D. La Rosa, R. Privitera (Eds.), Innovation in

Urban and Regional Planning, Springer International Publishing, 2021, pp. 427–438, https://doi.org/10.1007/978-3-030-68824-0_46.
[34] Z. Liu, W. Cheng, C.Y. Jim, T.E. Morakinyo, Y. Shi, E. Ng, Heat mitigation benefits of urban green and blue infrastructures: A systematic review of modeling techniques, validation and scenario simulation in ENVI-met V4, Build. Environ. 200 (2021), 107939, https://doi.org/10.1016/j.buildenv.2021.107939.
[35] J. Park, Y. Shin, S. Kim, S.-W. Lee, K. An, Efficient Plant Types and Coverage Rates for Optimal Green Roof to Reduce Urban Heat Island Effect, Sustainability 14 (4) (2022) Art. 4, https://doi.org/10.3390/su14042146.
[36] M. Ibrahim, Mitigation strategies of the urban heat island over Greater Cairo Metropolitan Area, Egypt utilizing ENVI-met model, Catrina: The International Journal of Environmental Sciences 0 (0) (2021) 35–47.
[37] H.M.P.I.K. Herath, R.U. Halwatura, G.Y. Jayasinghe, Modeling a Tropical Urban Context with Green Walls and Green Roofs as an Urban Heat Island Adaptation Strategy, Procedia Eng. 212 (2018) 691–698, https://doi.org/10.1016/j.proeng.2018.01.089.
[38] E. Shafiee, M. Faizi, S.-A. Yazdanfar, M.-A. Khanmohammadi, Assessment of the effect of living wall systems on the improvement of the urban heat island phenomenon, Build. Environ. 181 (2020) 106923.
[39] *ENVI-met—Decode urban nature with Microclimate simulations*. (n.d.). ENVI-Met. Retrieved May 12, 2022, from https://www.envi-met.com/.
[40] P.A. Mirzaei, Recent challenges in modeling of urban heat island, Sustain. Cities Soc. 19 (2015) 200–206, https://doi.org/10.1016/j.scs.2015.04.001.
[41] B.-J. He, J. Wang, J. Zhu, J. Qi, Beating the urban heat: Situation, background, impacts and the way forward in China, Renew. Sustain. Energy Rev. 161 (2022), 112350, https://doi.org/10.1016/j.rser.2022.112350.
[42] B.-J. He, J. Wang, H. Liu, G. Ulpiani, Localized synergies between heat waves and urban heat islands: Implications on human thermal comfort and urban heat management, Environ. Res. 193 (2021), 110584, https://doi.org/10.1016/j.envres.2020.110584.
[43] AWEKAS. (2020). *Dati archivio stazione Torino Ovest*. https://www.awekas.at/it/archiv.php?id=8986.
[44] Regione Lazio - ARSIAL. (2022). *SIARL Arsial: Dati agrometeorologici della Regione Lazio*. Regione Lazio. https://www.siarl-lazio.it/D5_ca.asp.
[45] ARPA Piemonte. (2020). *Dati meteoidrografici*. https://www.arpa.piemonte.it/rischinaturali/accesso-ai-dati/Richieste-dati-formato-standard/richiesta-dati/Richiesta-automatica/Dati-giornalieri-richiesta-automatica.html.
[46] Regione Lazio. (2017). *Rete Micrometeorologica*. https://dati.lazio.it/catalog/it/dataset/rete-micrometeorologica.
[47] *Geoportale Nazionale*. (n.d.). Retrieved April 20, 2021, from http://www.pcn.minambiente.it/viewer/.
[48] Resene. (n.d.). *Cool Colours | Colour Swatches | Resene Paints*. Retrieved December 18, 2020, from https://www.resene.co.nz/swatches/search.php?tofind=CoolColour+colours&submit3=List+colours&type=cool&page=.
[49] QGIS. (2022). *Benvenuto in QGIS!* https://qgis.org/it/site/.
[50] Comitato Termotecnico Italiano (CTI), Anni tipo climatici per applicazioni termotecniche, (n.d.). https://try.cti2000.it/ (accessed September 22, 2021).
[51] Ministero della Salute, Centro Nazionale Prevenzione e Controllo Malattie, Dipartimento di Epidemiologia SSR Regione Lazio. (2015). *Ondate di calore ed effetti sulla salute. Estate 2015. Sintesi dei risultati*. http://www.ccm-network.it/imgs/C_27_MAIN_page_1046_listaFile_List11_itemName_5_file.pdf.
[52] Ministero della Salute, Centro Nazionale Prevenzione e Controllo Malattie, Dipartimento di Epidemiologia SSR Regione Lazio. (2018). *Risultati dei Sistemi di allarme (HHWWS) e del Sistema di Sorveglianza della Mortalità Giornaliera (SiSMG) e degli accessi in pronto soccorso (15 maggio-15 settembre 2018). Sintesi dei risultati*. http://www.ccm-network.it/imgs/C_27_MAIN_page_1055_listaFile_List11_itemName_0_file.pdf.
[53] Regione Piemonte, & ARPA Piemonte. (2013). *Relazione sullo stato dell'ambiente in Piemonte*. https://www.regione.piemonte.it/web/sites/default/files/media/documenti/2018-10/pubblicazione_2013_web_parte1.pdf.
[54] A.A. Ghafar, I. Said, A.M. Fauzi, M.S. Shai-In, B. Jaafar, Comparison of leaf area index from four plant species on vertical greenery system in Pasir Gudang, Malaysia, Journal of Science and Technology 28 (2) (2020) 735–748.
[55] Europomice S.r.l., (n.d.). https://www.europomice.it/ (accessed April 19, 2021).
[56] A. Palla, I. Gnecco, L.G. Lanza, Unsaturated 2D modelling of subsurface water flow in the coarse-grained porous matrix of a green roof, J. Hydrol. 379 (1–2) (2009) 193–204, https://doi.org/10.1016/j.jhydrol.2009.10.008.
[57] N.K.C. Twarakavi, M. Sakai, J. Šimůnek, An objective analysis of the dynamic nature of field capacity, Water Resour. Res. 45 (10) (2009), https://doi.org/10.1029/2009WR007944.
[58] J. Li, B. Zheng, W. Shen, Y. Xiang, X. Chen, Z. Qi, Cooling and Energy-Saving Performance of Different Green Wall Design: A Simulation Study of a Block, Energies 12 (15) (2019) 2912, https://doi.org/10.3390/en12152912.
[59] Á. Szűcs, T. Gál, H. Andrade, Comparison of measured and simulated Mean Radiant Temperature: Case study in Lisbon (Portugal), Finisterra 49 (98) (2014) 95–111, https://doi.org/10.18055/Finis6469.
[60] Y.N. Ayyad, S. Sharples, Envi-MET validation and sensitivity analysis using field measurements in a hot arid climate, IOP Conference Series: Earth and Environmental Science 329 (1) (2019), 012040, https://doi.org/10.1088/1755-1315/329/1/012040.
[61] L. Bande, A. Afshari, D. Al Masri, M. Jha, L. Norford, A. Tsoupos, P. Marpu, Y. Pasha, P. Armstrong, Validation of UWG and ENVI-Met Models in an Abu Dhabi District Based on Site Measurements, Sustainability 11 (16) (2019) Art. 16, https://doi.org/10.3390/su11164378.
[62] M. Detommaso, V. Costanzo, F. Nocera, Application of weather data morphing for calibration of urban ENVI-met microclimate models, Results and critical issues. *Urban Climate* 38 (2021), 100895, https://doi.org/10.1016/j.uclim.2021.100895.
[63] S. Tsoka, K. Tsikaloudaki, T. Theodosiou, Coupling a Building Energy Simulation Tool with a Microclimate Model to Assess the Impact of Cool Pavements on the Building's Energy Performance Application in a Dense Residential Area, Sustainability 11 (9) (2019) Art. 9, https://doi.org/10.3390/su11092519.
[64] WMO. (2021). *Guide to Instruments and Methods of Observation (WMO-No. 8)* (2018th and 2021 editions ed.). WMO. https://library.wmo.int/index.php?id=12407&lvl=notice_display#.Y5cPTH3MK3A.
[65] G. Zhang, B.-J. He, Z. Zhu, B.J. Dewancker, Impact of Morphological Characteristics of Green Roofs on Pedestrian Cooling in Subtropical Climates, Int. J. Environ. Res. Public Health 16 (2) (2019) Art. 2, https://doi.org/10.3390/ijerph16020179.
[66] Milelli, M. (2016). *Urban heat island effects over Torino*. COSMO Newsletter No. 16. https://www.cosmo-model.org/content/model/documentation/newsLetters/newsLetter16/cnl16_01.pdf.
[67] G. Battista, L. Evangelisti, C. Guattari, E. De Lieto Vollaro, R. De Lieto Vollaro, F. Asdrubali, Urban Heat Island Mitigation Strategies: Experimental and Numerical Analysis of a University Campus in Rome (Italy), Sustainability 12 (19) (2020) Art. 19, https://doi.org/10.3390/su12197971.
[68] M. Zinzi, E. Carnielo, B. Mattoni, On the relation between urban climate and energy performance of buildings. A three-years experience in Rome, Italy, Applied Energy 221 (2018) 148–160, https://doi.org/10.1016/j.apenergy.2018.03.192.
[69] M.P. de Jesus, R.M. Lourenco, R.M. Arce, M. Marcias, Green façades and in situ measurements of outdoor building thermal behaviour—ScienceDirect, Build. Environ. 119 (2017) 11–19.
[70] M. Razzaghmanesh, M. Razzaghmanesh, Thermal performance investigation of a living wall in a dry climate of Australia, Build. Environ. 112 (2017) 45–62, https://doi.org/10.1016/j.buildenv.2016.11.023.
[71] N.H. Wong, A.Y. Kwang Tan, Y. Chen, K. Sekar, P.Y. Tan, D. Chan, K. Chiang, N. C. Wong, Thermal evaluation of vertical greenery systems for building walls, Build. Environ. 45 (3) (2010) 663–672, https://doi.org/10.1016/j.buildenv.2009.08.005.
[72] J. Iaria, T. Susca, Analytic Hierarchy Processes (AHP) evaluation of green roof- and green wall- based UHI mitigation strategies via ENVI-met simulations, Urban Clim. 46 (2022) 101293.
[73] O. Buchin, M.-T. Hoelscher, F. Meier, T. Nehls, F. Ziegler, Evaluation of the health-risk reduction potential of countermeasures to urban heat islands, Energ. Buildings 114 (2016) 27–37, https://doi.org/10.1016/j.enbuild.2015.06.038.
[74] C. Jin, X. Bai, T. Luo, M. Zou, Effects of green roofs' variations on the regional thermal environment using measurements and simulations in Chongqing, China, Urban For. Urban Green. 29 (2018) 223–237, https://doi.org/10.1016/j.ufug.2017.12.002.
[75] E. Ng, L. Chen, Y. Wang, C. Yuan, A study on the cooling effects of greening in a high-density city: An experience from Hong Kong, Build. Environ. 47 (2012) 256–271, https://doi.org/10.1016/j.buildenv.2011.07.014.
[76] T.E. Morakinyo, A. Lai, K.-K.-L. Lau, E. Ng, Thermal benefits of vertical greening in a high-density city: Case study of Hong Kong, Urban For. Urban Green. 37 (2019) 42–55, https://doi.org/10.1016/j.ufug.2017.11.010.
[77] Sahnoune, S., Benhassine, N., Bourbia, F., & Hadbaoui, H. (2021). Quantifying The Effect Of Green-Roof And Urban Green Infrastructure Ratio On Urban Heat Island Mitigation—Semi-Arid Climate. *QUANTIFYING THE EFFECT OF GREEN-ROOF AND URBAN GREEN INFRASTRUCTURE RATIO ON URBAN HEAT ISLAND MITIGATION - SEMI-ARID CLIMATE*. Scopus.
[78] J.A. Acero, E.J.Y. Koh, X. Li, L.A. Ruefenacht, G. Pignatta, L.K. Norford, Thermal impact of the orientation and height of vertical greenery on pedestrians in a tropical area, Build. Simul. 12 (2019) 973–984, https://doi.org/10.1007/s12273-019-0537-1.
[79] E. Alexandri, P. Jones, Temperature decreases in an urban canyon due to green walls and green roofs in diverse climates, Build. Environ. 43 (4) (2008) 480–493, https://doi.org/10.1016/j.buildenv.2006.10.055.
[80] C. He, J. Zhao, Y. Zhang, L. He, Y. Yao, W. Ma, P.L. Kinney, Cool Roof and Green Roof Adoption in a Metropolitan Area: Climate Impacts during Summer and Winter, Environ. Sci. Tech. 54 (17) (2020) 10831–10839, https://doi.org/10.1021/acs.est.0c03536.
[81] O. Lhotka, J. Kyselý, A. Farda, Climate change scenarios of heat waves in Central Europe and their uncertainties, Theor. Appl. Climatol. 131 (3) (2018) 1043–1054, https://doi.org/10.1007/s00704-016-2031-3.
[82] C. Gromke, B. Blocken, W. Janssen, B. Merema, T. van Hooff, H. Timmermans, CFD analysis of transpirational cooling by vegetation: Case study for specific meteorological conditions during a heat wave in Arnhem, Netherlands, Build. Environ. 83 (2015) 11–26, https://doi.org/10.1016/j.buildenv.2014.04.022.
[83] A. Wahid, S. Gelani, M. Ashraf, M.R. Foolad, Heat tolerance in plants: An overview, Environ. Exp. Bot. 61 (3) (2007) 199–223, https://doi.org/10.1016/j.envexpbot.2007.05.011.
[84] E.A. Waraich, R. Ahmad, A. Halim, T. Aziz, Alleviation of temperature stress by nutrient management in crop plants: A review, J. Soil Sci. Plant Nutr. 12 (2) (2012) 221–244, https://doi.org/10.4067/S0718-95162012000200003.
[85] J. Zhao, N. Meili, X. Zhao, S. Fatichi, Urban vegetation cooling potential during heatwaves depends on background climate, Environ. Res. Lett. (2022), https://doi.org/10.1088/1748-9326/acaf0f.Campbell, I., Sachar, S., Meisel, J., & Nanavatty, R. (2021). *Beating the heat: A sustainable Cooling Handbook for Cities*. UN environment programme.
[86] C. de Munck, G. Pigeon, V. Masson, F. Meunier, P. Bousquet, B. Tréméac, M. Merchat, P. Poeuf, C. Marchadier, How much can air conditioning increase air

temperatures for a city like Paris, France? Int. J. Climatol. 33 (1) (2013) 210–227, https://doi.org/10.1002/joc.3415.
[87] I. Campbell, S. Sachar, J. Meisel, R. Nanavatty, Beating the heat: A sustainable Cooling Handbook for Cities, (2021).
[88] Y. Zhao, S. Sen, T. Susca, J. Iaria, A. Kubilay, K. Gunawarden, X. Zhou, Y. Takane, Y. Park, X. Wang, A. Rubin, Y. Fan, C. Yuan, R. Bardhan, D. Derome, D. Ürge-Vorsatz, J. Carmeliet, Beating the Heat, Solution Sets for Developed Cities, 2023.